Available online at www.sciencedirect.com
ScienceDirect
Catalysis Today 137 (2008) 292–299
CATALYSIS TODAY
www.elsevier.com/locate/cattod

Role of vanadium sites in NO and O_2 adsorption processes over VO_x/CeO_2-ZrO_2 catalysts – EPR and IR studies

Andrzej Adamski [a,*], Barbara Gil [a], Zbigniew Sojka [a,b]

[a] *Jagiellonian University, Faculty of Chemistry, Ingardena 3, 30-060 Krakow, Poland*
[b] *Regional Laboratory of Physicochemical Analyses and Structural Research, Ingardena 3, 30-060 Krakow, Poland*

Available online 26 March 2008

Abstract

The interaction of NO and O_2 with 5 mol.% of vanadia deposited on $Ce_{0.10}Zr_{0.90}O_2$ and $Ce_{0.69}Zr_{0.31}O_2$ supports by wet impregnation was studied by means of EPR and IR. The supports were structurally characterized by XRD and Raman spectroscopy. Influence of the phase composition of the support on vanadium speciation as well as on surface architecture of the oxovanadium entities was discussed. The NO forms adsorbed on vanadium-containing systems were compared to those observed on bare CeO_2-ZrO_2 supports. The main products appearing on the catalysts surface during the consecutive reaction with NO and O_2 were identified and their thermal evolution was observed. Changes in vanadium speciation accompanying redox processes related to NO and O_2 activation were also observed and discussed.

Keywords: V_2O_5; CeO_2-ZrO_2; $deNO_x$; NO; IR

1. Introduction

Noxious character of NO_x emissions from stationary and mobile sources along with more restrictive regulations provide a sound incentive for extensive studies on development of efficient $deNO_x$ catalysts [1–3]. Nitrogen oxides (NO, NO_2 and N_2O), despite of being thermodynamically unstable ($\Delta_f G_{NO} = +86.55$ kJ/mol, $\Delta_f G_{NO_2} = +51.31$ kJ/mol, $\Delta_f G_{N_2O} = +104.2$ kJ/mol [4]), exhibit high kinetic durability due to the orbital symmetry and spin conservation barriers imposed on their direct decomposition into the constituent elements. Therefore, selective catalytic reduction remains at present the best practical way of NO_x removal from stationary sources [5,6], whereas, in the case of mobile sources, NO_x storage and reduction seems to be the best alternative, when the content of sulphur is relatively low [7,8]. Most of the promising results were obtained with catalysts based on transition metal oxides (TMOs) such as V_2O_5, WO_3 or MoO_3 [1,9,10]. The main advantage of such systems is their good structural stability and the possibility of functioning in relatively wide temperature window under variable redox conditions. Catalytic activity of TMOs in redox reactions, including NO_x abatement, can be increased by dispersion of the active oxide on supports of high specific surface area (TiO_2, Al_2O_3, ZrO_2, zeolites) [10–12]. The choice of an appropriate support is a very important issue, because the support oxide can strongly modify the structure of the deposited active phase, influencing catalytic properties of the investigated system in the similar extent as the type of applied reducing agent or the process conditions [10,13]. It is well known that ceria-zirconia binary oxides serve as excellent supports for noble metals in the three-way-catalysts (TWCs), being able to buffer fluctuations in the oxygen concentration owing to their high oxygen storage capacity (OSC) [14]. Binary CeO_2 and ZrO_2 oxides, calcined at temperatures above 600–700 °C, can easily form solid solutions in full concentration range, denoted hereafter as $Ce_yZr_{1-y}O_2$. Such systems may thus serve also as very promising supports for TMOs active in SCR and $deNO_x$ processes.

Supporting vanadia on CeO_2-ZrO_2 oxides results not only in better dispersion of the active phase but it also leads to a strong modification of the intrinsic properties of V_2O_5, enhancing its affinity to the reactants of $deNO_x$ process. Under real conditions, the catalyst works in the surplus of oxygen. In such a case, the reductive and oxidative properties of the

* Corresponding author. Tel.: +48 12 663 22 24; fax: +48 12 634 05 15.
E-mail address: adamski@chemia.uj.edu.pl (A. Adamski).

0920-5861/$ – see front matter © 2008 Elsevier B.V. All rights reserved.
doi:10.1016/j.cattod.2008.02.002

catalytic sites should be carfully optimized allowing for effective NO_x turnovers, even in the presence of injurious oxygen. It is thus reasonable to study the nature of specific electronic interactions between the catalytic centers and the deNO_x reactants in more detail. Especially important, from the mechanistic point of view, is establishing the boundary reaction conditions, in which strongly adsorbed surface intermediates are formed onto catalyst surface after NO_x introduction. Another vital task is spectroscopic determination of the chemical character of such intermediates, because their nature is a key parameter, decisive for the formation of reduced or oxidized nitrogen species, *i.e.* directly involved in NO_x abatement.

In the present work, interactions of $VO_x/Ce_yZr_{1-y}O_2$ (where $y = 0.10$ and 0.69) catalysts with NO were studied by EPR and IR techniques. Particular attention was devoted to the influence of the presence and structure of the deposited vanadia on NO activation modes and to the nature, thermal stability and transformation of reaction products in the presence of subsequently adsorbed oxygen.

2. Experimental

Ceria-lean and ceria-rich CeO_2-ZrO_2 supports, containing 10 and 69 mol.% of CeO_2, respectively, were supplied by *Rhodia* (France). The samples were obtained from nitrate precursors by hydrothermal synthesis. Fresh preparations were dried at 373 K for 1 h in air and then calcined at 873 K for 6 h. Specific surface areas, determined by the N_2-BET method, were equal to 73 m^2/g in the case of $Ce_{0.10}Zr_{0.90}O_2$ and 124 m^2/g for $Ce_{0.69}Zr_{0.31}O_2$ system.

Catalysts containing 5 mol.% of V_2O_5 (labeled hereafter 5V/support) were prepared by wet impregnation of the corresponding $Ce_yZr_{1-y}O_2$ carriers with an appropriate amount of aqueous solution of ammonium metavanadate (NH_4VO_3, *Merck* 99.9%). The samples were next dried at 373 K for 12 h and calcined in air at 873 K for 6 h.

XRD measurements were performed with the 0.5°/min steps in the 2Θ range of 20–70° using a DRON-3 diffractometer and Ni-filtered CuKα radiation (λ = 1.5408 Å). The phase composition of the samples was calculated from the following relationships:

$$X_t = I_t(1\,1\,1)/[I_t(1\,1\,1) + I_m(1\,1\,1) + I_m(1\,1\,\bar{1})], \quad X_m = 1 - X_t \tag{1}$$

where X_t and X_m stand for the fraction of the tetragonal and the monoclinic polymorph of ZrO_2, respectively, whereas I_t and I_m are the intensities of their diagnostic peaks [15].

Raman spectra were registered with FTS 6000 spectrometer equipped with a BIORAD accessory. The samples were excited with the 1064 nm line of a diode-pumped Nd:YAG laser (Spectra Physics Model T108S), and the scattered radiation was collected at 180° with 4 cm^{-1} resolution. The IR spectra were registered with the resolution of 2 cm^{-1} using an Equinox 55 spectrometer equipped with a MCT detector. The samples placed in the IR cell on a silicon wafer were treated *in situ*. The X-band CW-EPR spectra were recorded at room and liquid nitrogen temperatures with a Bruker ELEXSYS E-500 spectrometer operating at the 100 kHz field modulation. EPR parameters were determined by simulation using the EPRsim32 program [16].

Nitric oxide was adsorbed at the pressures of 2–20 Torr (non-equilibrium conditions) on the samples previously outgassed at $p \leq 10^{-5}$ Torr, and thermally activated at 623–673 K for 0.5 h. The samples were contacted with NO at 77 K for 2 min and next gradually exposed to room (RT) or more elevated temperatures, to follow the adsorption progress monitored by EPR or IR. Once the NO evolution was accomplished, the samples were outgassed and oxygen was introduced under the pressure of 13–15 Torr at 77 K.

3. Results and discussion

3.1. Phase composition of $VO_x/Ce_yZr_{1-y}O_2$ catalysts

Understanding the nature of the interaction between the binary CeO_2-ZrO_2 supports and the deposited V_2O_5 requires a more in-depth phase analysis of both carriers and the final catalysts. At room temperature monoclinic (*m*) polymorph of

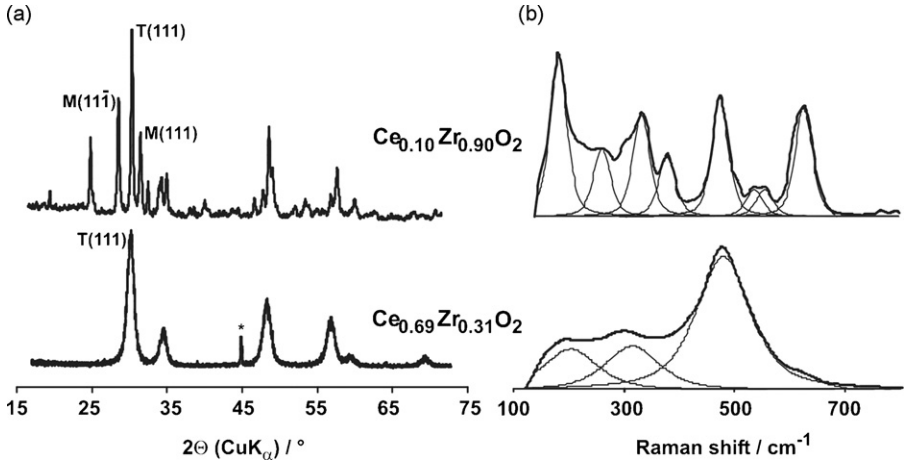

Fig. 1. XRD patterns (a) and deconvoluted Raman spectra (b) of the $Ce_{0.10}Zr_{0.90}O_2$ and $Ce_{0.69}Zr_{0.31}O_2$ supports (*a maximum from an XRD holder).

zirconia is thermodynamically stable. Introduction of 10 and 69 mol.% of ceria to zirconia, accompanying formation of the corresponding solid solutions, results in partial or total stabilization of the tetragonal polymorph (*t*), as it can be inferred from the corresponding XRD patterns (Fig. 1a). It is well known that ceria additives can efficiently stabilize at room temperature the high-temperature *t*-ZrO_2 polymorph [14,17]. An increase of CeO_2 content in the binary system from 10 to 69 mol.% led to the disappearance of two characteristic maxima, corresponding to (1 1 1) and $(1\,1\,\bar{1})$ Bragg reflexions, diagnostic of the monoclinic zirconia phase. The content of the monoclinic phase in $Ce_{0.10}Zr_{0.90}O_2$, evaluated from the integral intensity of the corresponding reflections according to Eq. (1), was equal to 54% and then dropped to zero for $Ce_{0.69}Zr_{0.31}O_2$. In turn, a single (1 1 1) Bragg maximum, diagnostic of the tetragonal phase, predominated the XRD pattern in the case of $Ce_{0.69}Zr_{0.31}O_2$ support. Since the metastable tetragonal phase can exist in two t' and t'' variants of slightly different oxygen arrangement, depending on the CeO_2 content [18], distinguishing between them is easier basing on the Raman spectra (Fig. 1b). The latter are more sensitive to the short-range oxygen displacement, owing to the large polarizability of oxygen ions. As calcination temperature was moderate (600 °C), which resulted in rather low crystallinity of the studied samples, formation of the $Ce_yZr_{1-y}O_2$ solid solutions does not exclude the presence of CeO_2- and ZrO_2-rich nanodomains, which cannot be detected by both XRD and RS methods [19,20].

The factor group theoretical analysis predicts 18 ($9A_g + 9B_g$) Raman-active modes for the monoclinic ZrO_2 form and 6 ($A_{1g} + 2B_{1g} + 3E_g$) for the tetragonal one [21,22]. The number of components observed in the Raman spectra presented in Fig. 1b decreased with CeO_2 loading, from at least 8 bands observable for $Ce_{0.10}Zr_{0.90}O_2$ ($m + t'$) to 4 for $Ce_{0.69}Zr_{0.31}O_2$ (t''). The spectra of the investigated supports differed in the number of the resolved bands, however in both cases the intense bands occurring at 486 and 474 cm^{-1} for $Ce_{0.10}Zr_{0.90}O_2$ and $Ce_{0.69}Zr_{0.31}O_2$, respectively, can be attributed to the symmetrical F_{2g} mode in the fluorite-like structure, revealing clearly the presence of the metastable tetragonal phases. For the $Ce_{0.69}Zr_{0.31}O_2$ support, both the shape and the position of the corresponding spectral lines univocally confirm the presence of the t'' polymorph [18]. A more detailed interpretation of the Raman spectra of the $Ce_yZr_{1-y}O_2$ systems can be found elsewhere [23].

A shoulder at 540 cm^{-1} visible in the Raman spectrum of the $Ce_{0.10}Zr_{0.80}O_2$ solid solution was most probably due to luminescence of a trivalent lanthanide impurity. Such impurities are often present in ceria-zirconia materials and can strongly influence Raman spectra [24].

Deposition of 5 mol.% of V_2O_5 on the surface of the $Ce_{0.10}Zr_{0.90}O_2$ and $Ce_{0.69}Zr_{0.31}O_2$ carriers did not entail any distinct changes in the phase composition of the investigated systems. No traces of crystalline vanadia were observed in the XRD patterns recorded for both catalysts. Also in the Raman spectra any new feature did not appear below 750 cm^{-1} (the diagnostic region of the $Ce_yZr_{1-y}O_2$ matrix), as it can be seen for the 5 $V/Ce_{0.69}Zr_{0.31}O_2$ sample in Fig. 2. However, above 750 cm^{-1} new weak bands, characteristic of cerium orthovanadate ($CeVO_4$) can be distinguished. The latter can be formed according to the solid state reaction:

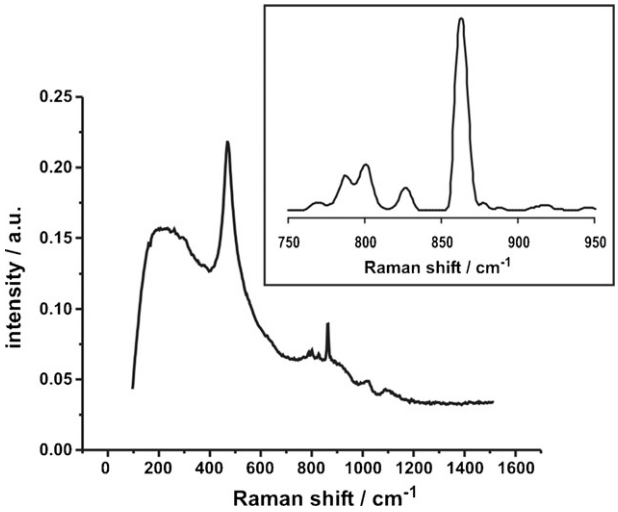

Fig. 2. Raman spectrum of the $5V/Ce_{0.69}Zr_{0.31}O_2$ catalyst. In the insert, an enlarged region diagnostic for $CeVO_4$ vibrations is shown.

$$V_2O_5 + 2CeO_2 = 2CeVO_4 + \tfrac{1}{2}O_2 \quad (2)$$

Apparently, the quantity of $CeVO_4$ was too small to be detected by XRD. The formation of $CeVO_4$ for ceria and ceria-zirconia-supported vanadia catalysts was also observed by other authors at similar calcination conditions [25–27].

The enlarged fragment of the Raman spectrum diagnostic of $CeVO_4$ is shown in the insert in Fig. 2. The most pronounced band at 858 cm^{-1}, together with the two weaker ones around 800 cm^{-1}, can be attributed to the A_{1g} symmetric and to the E_g and B_{2g} antisymmetric stretchings of the vanadates, respectively [28]. Obviously, the presence of such a product was more pronounced in the case of $5V/Ce_{0.69}Zr_{0.31}O_2$, where higher ceria content favored $CeVO_4$ formation, than in the case of the $5V/Ce_{0.10}Zr_{0.90}O_2$ sample. The lack of any bands due to surface oxovanadium species in the Raman spectra of the $5V/Ce_yZr_{1-y}O_2$ system, regardless the phase composition of the carrier, suggested that in both cases the VO_x species can undergo preferential reaction with CeO_2 component of the support to form the orthovanadate phase.

3.2. Vanadium speciation

Deposition of V_2O_5 on both $Ce_{0.10}Zr_{0.90}O_2$ and $Ce_{0.69}Zr_{0.31}O_2$, supports led to a distinct decrease of the specific surface area of the resultant catalysts from 73 to 34 cm^2/g and from 124 to 52 cm^2/g, respectively. This can be regarded as a proof of the specific interaction between deposited phase and CeO_2-ZrO_2 supports.

It is known that thermal treatment of supported vanadia catalysts results in non-stoichiometry of the deposited phase due to partial reduction of vanadium, even in the presence of oxygen [29]. This fact can be related to the strong interaction

between the deposited phase and the support leading to formation of a solid solution [30], according to the equation

$$xV_2O_5 + MeO_2 = 2V_xMe_{1-x}O_2 + xO_2, \quad \text{where Me} = \text{Ce, Zr}. \tag{3}$$

Such process has to be accompanied by a reduction of V^{5+} to V^{4+}, favored by isovalent substitution. In consequence, the reduced vanadium ions can easily migrate into the bulk of the matrix, forming the corresponding solid solution. Surprisingly, only in the case of $5V/Ce_{0.10}Zr_{0.90}O_2$ the EPR spectrum revealed a weak signal from the paramagnetic V^{4+} ($3d^1$) ions with traces of the hyperfine structure, originating from the interaction of the unpaired electron with the ^{51}V nucleus ($I = 7/2$, 99.76%), whereas the $5V/Ce_{0.69}Zr_{0.31}O_2$ sample was almost EPR silent. Evidently, the majority of vanadium(V) stabilized as diamagnetic cerium orthovanadate was reluctant to reduction. Recently, Aboukaïs and co-workers confirmed that indeed, reducibility of $CeVO_4$ is distinctly lower than that of V_2O_5 [31]. Heating of both samples at 973 K for 0.5 h resulted in the appearance of stronger, quite complex EPR spectra (Fig. 3). The differences in the shape of the recorded signals clearly reflected different status of V^{4+} ions in the samples with ceria-lean and ceria-rich supports. The hyperfine structure of the $5V/Ce_{0.10}Zr_{0.90}O_2$ spectrum with $|A_1| = 15.98$, $|A_2| = 7.24$ and $|A_3| = 3.19$ mT was characteristic of V^{4+} ions stabilized within the bulk [32], whereas in the case of $5V/Ce_{0.69}Zr_{0.31}O_2$ two types of overlapping hyperfine patterns due to the bulk and surface V^{4+} can be distinguished. This indicated that in the latter case, only a part of tetravalent vanadium was incorporated in CeO_2-ZrO_2 matrix, and the rest remained on the catalysts surface. Computer simulations confirmed the presence of heterogeneous V^{4+} centers, contributing to the spectra presented in Fig. 3. Beside the oxovandium species isolated on the support surface, giving rise to an axial signal with the 8-line hyperfine structure, magnetically interacting, polymeric V_xO_y entities were also found being responsible for the broad structureless signals. An orthorhombic component with the clearly resolved hyperfine structure was attributed to the V^{4+} ions isolated within the CeO_2-ZrO_2 matrix. The parameters of all EPR signals are summarized in Table 1. The relative ratio of the isolated to the polymeric surface V^{4+} sites and to the V^{4+} ions stabilized within the matrix was found to be 12%:38%:50% for $5V/Ce_{0.10}Zr_{0.90}O_2$ and 17%:56%:27% for $5V/Ce_{0.69}Zr_{0.31}O_2$ samples, reflecting distinct influence of the phase composition of the support on the speciation of vanadium ions. It is quite characteristic that higher ceria content in the support composition favored the formation of the polymeric vanadium surface species and prevented V^{4+} ions from their migration to the bulk. Both observations can be related to the formation of surface vanadates, which are more resistant to spontaneous reduction.

3.3. NO adsorption

Low-temperature (77 K) adsorption of 20 Torr of NO on bare $Ce_{0.10}Zr_{0.90}O_2$ sample and its subsequent exposure to room temperature led to the appearance of a weak signal typical of loosely trapped NO molecules with the barely resolved ^{14}N hyperfine structure ($I = 1$, 99.63%) (Fig. 4A-a), whereas in the case of the $Ce_{0.69}Zr_{0.31}O_2$ support, the observed EPR signal was assigned to nitrosyl complexes (Fig. 4A-b). The presence of weakly adsorbed NO on $Ce_{0.10}Zr_{0.90}O_2$ at 173 K was confirmed by the IR band at 1850 cm^{-1}, ascribed to ν_{N-O} stretching in free NO molecule, where the characteristic P, Q, R branches were visible [33] (Fig. 4B-a). The strong IR band at 1750 cm^{-1} in the spectrum of NO interacting with $Ce_{0.69}Zr_{0.31}O_2$ (Fig. 4B-b) indicated that NO molecules were adsorbed in the bent mode, acquiring some partial negative charge ($NO^{\delta-}$), typical of surface-stabilized mononitrosyls [34]. The occurrence of additional weak bands at 1185–1195 cm^{-1} confirmed also the formation of a small quantity of strongly bent or even bridging (η^2-N,O) nitrosyl species [34]. More detailed description of NO adsorption on bare CeO_2-ZrO_2 supports was reported elsewhere [23]. The obtained results remain in good agreement with previous results published by the other authors [35,36].

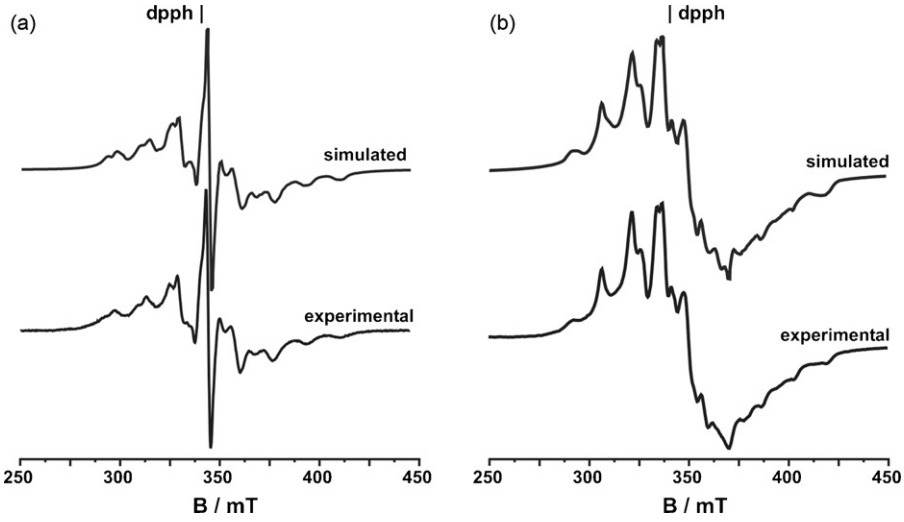

Fig. 3. Simulated and experimental EPR spectra recorded at 77 K of (a) $5V/Ce_{0.10}Zr_{0.90}O_2$ and (b) $5V/Ce_{0.69}Zr_{0.31}O_2$, thermally treated at 973 K.

Table 1
Average parameters obtained by computer simulation for EPR spectra of $5V/Ce_yZr_{1-y}O_2$ samples (presented in Fig. 3) and their assignment to the corresponding paramagnetic species

Type of V^{4+} species	EPR parameter	$5V/Ce_{0.10}Zr_{0.90}O_2$	$5V/Ce_{0.69}Zr_{0.31}O_2$
Isolated on the surface	$g_{\|\|}$	1.926	1.923
	$g_{\perp}$	1.977	1.972
	$\|A_{\|\|}\|$ (mT)	16.34	16.90
	$\|A_{\perp}\|$ (mT)	6.88	6.44
Interacting in surface polymers	$g_{\|\|}$	1.941	1.945
	$g_{\perp}$	1.968	1.966
Isolated within the matrix	g_1	1.900	1.880
	g_2	1.968	1.951
	g_3	1.943	1.931
	$\|A_1\|$ (mT)	15.98	15.61
	$\|A_2\|$ (mT)	7.24	7.44
	$\|A_3\|$ (mT)	3.19	1.96

Contrary to the results of NO interaction with the bare matrices, no paramagnetic nitrosyl species were detected by EPR after adsorption of 2–3 Torr of nitric oxide on both $5V/Ce_{0.10}Zr_{0.90}O_2$ and $5V/Ce_{0.69}Zr_{0.31}O_2$ samples at 77 K. Evolution of the EPR spectra of the NO_x-$5V/Ce_{0.69}Zr_{0.31}O_2$ complexes induced by their exposure to ambient conditions is shown in Fig. 5A. Analogous evolution for the $Ce_{0.10}Zr_{0.90}O_2$ sample was less informative, as the part of the V^{4+} ions was stabilized within the matrix and thus remained inaccessible to NO. The intensity of the EPR spectrum due to vanadium(IV) increased about 2.5 times upon NO admission (Fig. 5A-a and b). After slight fluctuations it was maintained during the next 10 min of the sample exposure to room temperature, as shown in the insert in Fig. 5A. Exposure of the sample to 343 and next to 573 K caused a pronounced decrease in the abundance of the vanadium(IV) species (Fig. 5A-d and e). The observed changes can be explained by a two-step thermally activated reduction of vanadium sites, $V^{5+} \rightarrow V^{4+} \rightarrow V^{3+}$, by the adsorbed nitric oxide. Deeply reduced vanadium forms were insensitive to admission of the next portion of 20 Torr of NO at ambient or elevated temperatures. Along with changes in the content of the EPR-active V^{4+} ions, the evolution of vanadium speciation was also observed. The amount of clustered vanadium entities was distinctly higher after NO interaction with the catalysts surface at 573 K, whereas the amount of the isolated V^{4+} species on the $Ce_{0.69}Zr_{0.31}O_2$ surface decreased by 32%, as revealed by the computer simulation. Possible explanation of this fact can be associated with oxygen extraction from the coordination sphere of vanadium by the NO ligand undergoing oxidation. The resultant oxygen deficit can be compensated by the higher agglomeration of oxovandium forms [37], structurally corresponding to the tranformation of VO_2 into V_2O_3.

It is generally accepted basing on the previous IR results, that NO does not adsorb over fully oxidized oxide-supported vanadia surfaces [10,38,39]. Our samples, however, were partally reduced as it was confirmed by the presence of the corresponding EPR signal from V^{4+}. IR spectra recorded after NO admission onto $5V/Ce_yZr_{1-y}O_2$ catalysts showed that, regardless the phase composition, in our case the main products of surface reaction were diamagnetic nitrates and nitrites, formed already at 173 K, as it can be seen in the spectrum for $5V/Ce_{0.69}Zr_{0.31}O_2$ presented in Fig. 5B. The band at 1585 cm^{-1} can be attributed to the asymmetric ν_{NO_2} vibrations in O–NO_2^- or bridging NO_3^- forms, whereas the two bands at 1250–1290 cm^{-1} were ascribed to the symmetric ν_{NO_2} modes of NO_2^- or bridging NO_3^- [33,34,40]. Apart from the NO

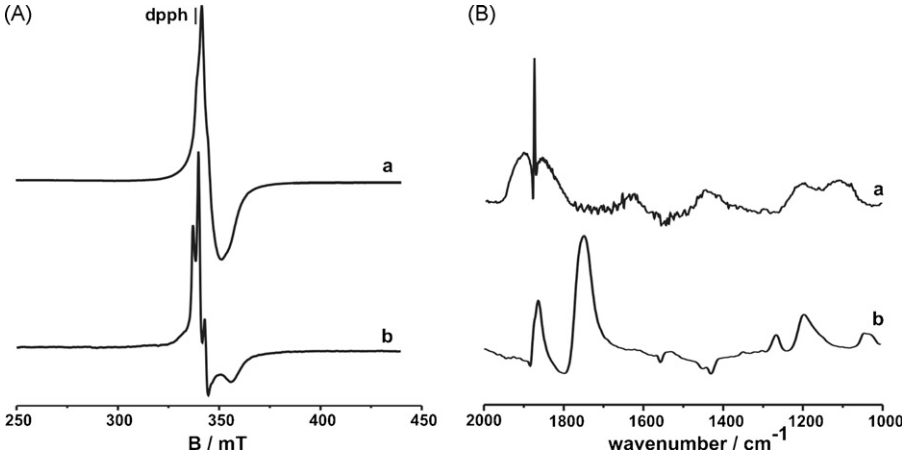

Fig. 4. EPR spectra (A), and IR spectra (B) of (a) $Ce_{0.10}Zr_{0.90}O_2$ and (b) $Ce_{0.69}Zr_{0.31}O_2$ catalysts after NO adsorption (p_{NO} = 20 Torr) at 77 and 173 K, respectively.

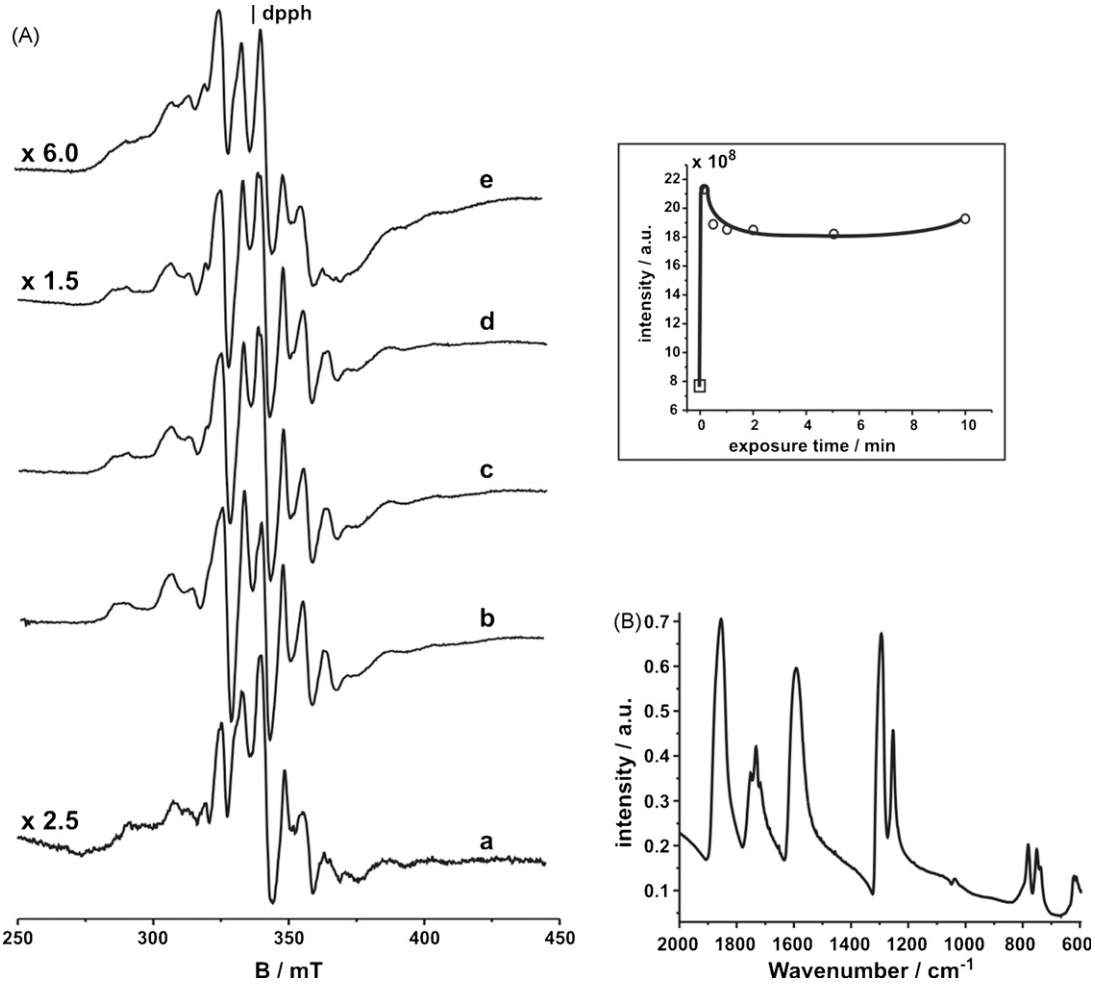

Fig. 5. (A) Sequence of EPR spectra (recorded at 77 K) of 5V/$Ce_{0.69}Zr_{0.31}O_2$ calcined at 873 K (a) before NO adsorption, (b) just after NO admission at 77 K and p_{NO} = 7 Torr, after 10 min of exposure to (c) room temperature, (d) 343 K, and (e) 573 K. In the insert, changes in the spectrum intensity as a function of exposure time to RT is shown. Point (□) stands for the intensity before NO introduction. (B) IR spectrum of NO (p_{NO} = 10 Torr) adsorbed on 5V/$Ce_{0.69}Zr_{0.31}O_2$ sample at 173 K.

oxidation products, traces of nitrosyls (ν_{N-O} at 1730 cm^{-1}), N_2O_4 dimers (with several deformation modes around 750 cm^{-1}), along with the physisorbed NO (ν_{N-O} at 1850 cm^{-1}) contributed to the IR spectrum.

3.4. Oxygen adsorption

Introduction of oxygen ($p_{O_2} = 13 - 15$ Torr, $T = 77$ K) onto the surface of 5V/$Ce_yZr_{1-y}O_2$ with preadsorbed NO, led to reappearance of the EPR signal due to surface V^{4+} ions for both studied samples (Fig. 6A and B). Intensity of the EPR spectra just after O_2 adsorption was however distinctly lower than before oxygen admission (Fig. 6A and B-a). Evidently, even low-temperature interaction of vanadium sites with O_2 can led to their reoxidation. Strongly reduced sites were first oxidized to the paramagnetic V^{4+}, giving rise to the observed changes in shape and structure of the recorded spectra (Fig. 6A and B-a), whereas the residual V^{4+} species underwent oxidation to V^{5+} becoming EPR silent. Simultaneously the new intense orthorhombic signal appeared in the EPR spectra (marked with an arrow in Fig. 6A and B). Its shape and EPR parameters (g_1 = 2.102, g_2 = 2.088 and g_3 = 2.071) can be attributed to the paramagnetic superoxide O_2^- ($^2\Pi_{3/2}$) anion radicals [41]. Such radicals can also be formed on pure CeO_2-ZrO_2 supports, but their EPR parameters were slightly different (g_1 = 2.012, g_2 = 2.018 and g_3 = 2.037) [42].

Formation of O_2^- on the surface required an electron transfer from the vanadium(IV) ion to the adsorbed dioxygen molecule, according to the equation: $O_2 + V^{4+} = V^{5+}-O_2^-$. In consequence a partial decrease in the intensity of the V^{4+} signal can be observed. Intensity of the signal due to the O_2^- radicals slightly increased with the temperature and was the highest after keeping the samples at 723 K for 10 min (Fig. 6 A and B-b). Changes in vanadium status just after dioxygen introduction and subsequent evolution in the intensity of the EPR signals of both V^{4+} and O_2^- revealed rather fast O_2 activation, *via* metal-to-ligand electron transfer (MLET).

Formation of surface O_2^- species remains of vital importance for deNO_x chemistry, because they can react directly with NO molecules from the gas phase (according to the Rideal-Eley mechanism) to form diamagnetic NO_3^- as the final products of surface reaction.

In the IR spectra recorded after O_2 admission onto NO_x-5V/$Ce_yZr_{1-y}O_2$ sample, an increase in the intensity of

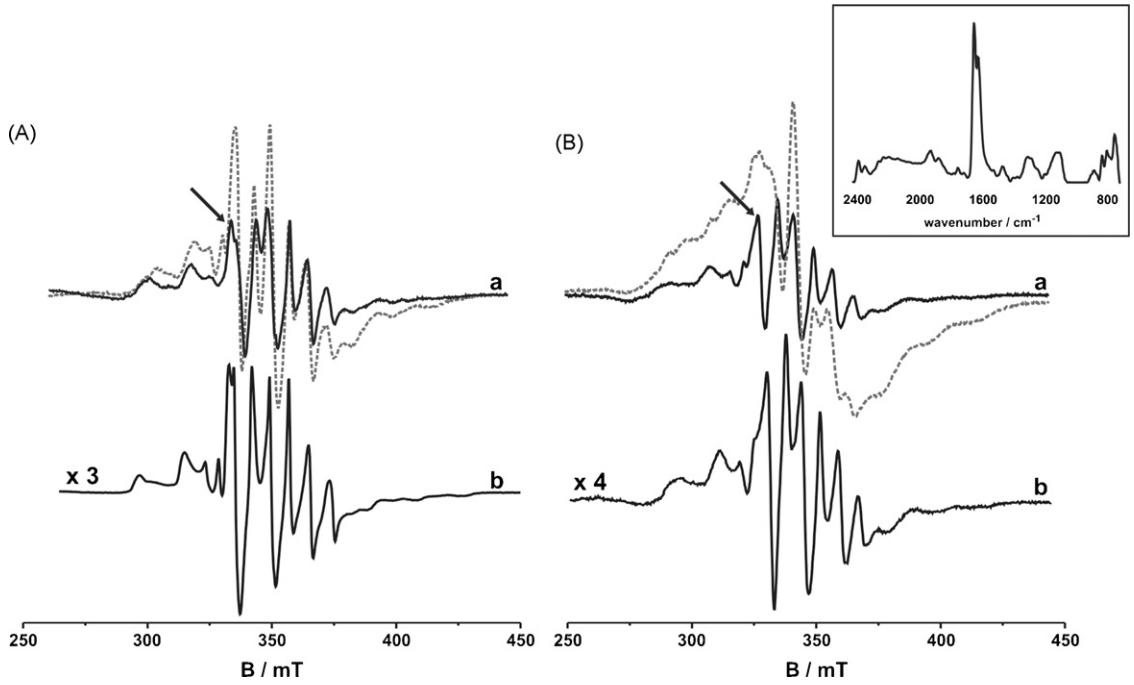

Fig. 6. EPR spectra (recorded at 77 K) of NO-treated (A) 5V/$Ce_{0.10}Zr_{0.90}O_2$ and (B) 5V/$Ce_{0.69}Zr_{0.31}O_2$ systems (a) solid line—before O_2 adsorption, dashed line—just after O_2 adsorption (p_{O_2} = 13 − 15 Torr, 77 K) and (b) heating to 723 K. In the insert, IR spectrum of 5V/$Ce_{0.69}Zr_{0.31}O_2$ after consecutive NO (p_{NO} = 10 Torr) and O_2 (p_{O_2} = 20 Torr) adsorption is shown.

the bands assigned to surface nitrates was observed, as it can be seen for 5V/$Ce_{0.69}Zr_{0.31}O_2$ in the insert to Fig. 6. Surface nitrates formed during interaction with O_2 were more abundant and slightly different in nature than those observed on the same sample in the absence of oxygen. The most abundant monodentate NO_3^- species, contributed to the strong bands around 1600 cm^{-1}, ascribed to the asymmetric ν_{NO_2} vibrations [34]. Similar products were observed after the joined interaction of NO and O_2 with zirconia-supported vanadia also by other authors [43].

4. Conclusions

Deposition of 5 mol.% of vanadia onto the monoclinic or tetragonal CeO_2-ZrO_2 supports distinctly altered their reactivity toward NO at low and medium temperatures. Weakly physisorbed NO or chemisorbed nitrosyl forms, dominated over the bare $Ce_{0.10}Zr_{0.90}O_2$ and $Ce_{0.69}Zr_{0.31}O_2$ samples, respectively, whereas oxidized products (nitrites and nitrates) were found after NO adsorption on 5V/$Ce_yZr_{1-y}O_2$ catalysts. Simultaneously, vanadium sites were reversibly reduced. Reaction of 5V/$Ce_yZr_{1-y}O_2$ with NO led not only to changes in the oxidation state of surface vanadium ions but also to changes in their speciation, resulting in higher population of more agglomerated reduced oxovanadium forms. Subsequent O_2 adsorption on 5V/$Ce_yZr_{1-y}O_2$ with preadsorbed NO led to the partial reoxidation of surface vanadium sites and to the formation of O_2^- radicals, accompanied by the formation of surface nitrates.

Distribution of vanadium between surface and bulk, as well as heterogeneity of surface vanadium sites were affected by the phase composition of the support. At ceria content of 69 mol.%, vanadium was stabilized on the catalysts surface mainly in polymeric forms, preserving active sites from migration into the matrix, whereas in the case of 5V/$Ce_{0.10}Zr_{0.90}O_2$, relatively large amount of vanadium ions was stabilized within the bulk and thus remain inaccessible to the reactants from the gas phase.

Acknowledgements

The authors are grateful to Dr. A. Wesełucha-Birczyńska from Regional Laboratory of Physicochemical Analyses and Structural Research for recording the Raman spectra and to K. Sadowska and A. Pietruszka, the students working with A. Ad. for their help in preparing the samples. The work was realized in the framework of the project PBZ-MEiN-3/2/2006.

References

[1] P. Forzatti, Appl. Catal. A 222 (2001) 221.
[2] M. Iwamoto, Stud. Surf. Sci. Catal. 130 (2000) 23.
[3] J.N. Armor, in: J.N. Armor (Ed.), Enivironmental Catalysis, ASC Symp. Series, vol. 552, ACS, Washington, 1994.
[4] P.W. Atkins, Physical Chemistry, PWN, Warsaw, 2001, Polish edition.
[5] E. Jobson, Top. Catal. 28 (2004) 191.
[6] R. Burch, J.P. Breen, F.C. Meunier, Catal. Today 90 (2004) 27.
[7] M. Takeuchi, Sh. Matsumoto, Top. Catal. 28 (2004) 151.
[8] Z. Liu, S.I. Woo, Catal. Rev. - Sci. Eng. 48 (2006) 43.
[9] B.M. Weckhuysen, D.E. Keller, Catal. Today 78 (2003) 25.
[10] G. Busca, L. Lietti, G. Ramis, F. Berti, Appl. Catal. B 18 (1998) 1.
[11] K. Bourikas, Ch. Fountzoula, Ch. Kordulis, Appl. Catal. B 52 (2004) 145.
[12] Y. Habuta, N. Narishige, K. Okumura, N. Katada, M. Niwa, Catal. Today 78 (2003) 131.

[13] G. Djéga-Mariadassou, Catal. Today 90 (2004) 27.
[14] A. Trovarelli (Ed.), Catalysis by Ceria and Related Materials, Imperial College Press, London, 2002.
[15] P.D.L. Mercera, J.G. van Ommen, E.B.M. Doesburg, A.J. Burggraaf, J.H.R. Ross, Appl. Catal. 57 (1990) 127.
[16] T. Spalek, P. Pietrzyk, Z. Sojka, J. Chem. Inf. Model. 45 (2005) 18.
[17] M. Fernández-García, A. Martínez-Arias, J.C. Hanson, J.A. Rodriguez, Chem. Rev. 104 (2004) 4063.
[18] M. Yashima, H. Arashi, M. Kakihana, M. Yoshimura, J. Am. Ceram. Soc. 77 (1994) 1067.
[19] E. Mamontov, R. Brezny, M. Koranne, T. Egami, J. Phys. Chem. B 107 (2003) 13007.
[20] R. Di Monte, J. Kašpar, J. Mater. Chem. 15 (2005) 633.
[21] T. Hirata, E. Asari, M. Kitajima, J Solid State Chem. 110 (1994) 201.
[22] V. Sánchez-Escribano, E. Fernández-López, M. Panizza, C. Resini, J.-M. Gallardo-Amores, G. Busca, Solid State Sci. 5 (2003) 1369.
[23] A. Adamski, E. Tabor, B. Gil, Z. Sojka, J. Catal. Today 119 (2007) 114.
[24] P. Fornasiero, A. Speghini, R. Di Monte, M. Bettinelli, J. Kašpar, A. Bigotto, V. Sergo, M. Graziani, Chem. Mater. 16 (2004) 1938.
[25] B.M. Reddy, P. Lakshmanan, A. Khan, C. López-Cartes, T.C. Rojas, A. Fernández, J. Phys. Chem. B 109 (2005) 1781.
[26] B.M. Reddy, P. Lakshmanan, S. Loridant, Y. Yamada, T. Kobayashi, C. López-Cartes, T.C. Rojas, A. Fernández, J. Phys. Chem. B 109 (2005) 1781.
[27] W. Daniell, A. Ponchell, S. Kuba, F. Anderle, T. Weingand, D.H. Gregory, H. Knőzinger, Top. Catal. 20 (2002) 65.
[28] M.V. Martínez-Huerta, J.M. Coronado, M. Fernández-García, A. Iglesias-Juez, G. Deo, J.L.G. Fierro, M.A. Bañares, J. Catal. 225 (2004) 240.
[29] M. Schraml-Marth, A. Wokaun, A. Baiker, J. Catal. 124 (1990) 86.
[30] G. Centi, E. Giamello, D. Pinelli, F. Trifiró, J. Catal. 130 (1991) 220.
[31] E. Abi-Aad, J. Matta, D. Courcot, A. Aboukaïs, J. Mater. Sci. 41 (2006) 1827.
[32] A. Adamski, Z. Sojka, K. Dyrek, M. Che, S. Albrecht, G. Wendt, Langmuir 15 (1999) 5733.
[33] A.A. Davydov, Infrared Spectroscopy of Adsorbed Species on the Surface of Transition Metal Oxides, John Wiley & Sons, Chichister/New York/Brisbane/Toronto/Singapore, 1990.
[34] K.I. Hadjiivanov, Catal. Rev. - Sci. Eng. 42 (2000) 71.
[35] P. Fornasiero, J. Kašpar, Collect. Czech. Chem. Commun. 66 (2001) 1287.
[36] M. Haneda, T. Morita, Y. Nagao, Y. Kintaichi, H. Hamada, PCCP 3 (2001) 4696.
[37] J. Haber, A. Kozłowska, R. Kozłowski, J. Catal. 102 (1986) 52.
[38] I. Nova, L. Lietti, E. Tronconi, P. Forzatti, Catal. Today 60 (2000) 73.
[39] M.A. Centeno, I. Carrizosa, J.A. Odrizola, Appl. Catal. B 29 (2001) 307.
[40] G. Ramis, G. Busca, F. Bregani, P. Forzatti, Appl. Catal. 64 (1990) 259.
[41] M. Che, A. Tench, Adv. Catal. 32 (1983) 1.
[42] A. Adamski, G. Djéga-Mariadassou, Z. Sojka, Catal. Today 119 (2007) 120.
[43] G. Ghiotti, F. Prinetto, Res. Chem. Intermed. 25 (1999) 131.